ISSN 0869-5911, Petrology, 2024, Vol. 32, No. 2, pp. 165–178. © The Author(s), 2024. This article is an open access publication.

Paleoproterozoic Dacite Dikes of the Vorontsovka Terrane, Volga–Don Orogen: Geochemistry, Age, and Petrogenesis

K. A. Savko[a, *], A. V. Samsonov[b], E. Kh. Korish[a], N. S. Bazikov[a], and A. N. Larionov[c]

[a] *Voronezh State University, Voronezh, Russia*

[b] *Institute of Geology of Ore Deposits, Petrography, Mineralogy and Geochemistry, Russian Academy of Science, Moscow, Russia*

[c] *Center for Isotope Research, Karpinsky Russian Geological Research Institute, St. Petersburg, Russia*

**e-mail: ksavko@geol.vsu.ru*

Received May 10, 2023; revised September 13, 2023; accepted October 19, 2023

Abstract—Metamorphosed dacitic porphyry dikes were first found in the western part of the Vorontsovka terrane, which is located in the Paleoproterozoic Volga–Don orogen at the margin of Archean Sarmatia and Volga–Ural cratons. The magmatic protolith age for the metadacites is ca. 2.07 Ga. These are ferrous, metaluminous calc-alkali I-type granitoids. The sodium specialization of the rocks and their low concentrations of Mg, Cr, Ni, and incompatible elements, with significant REE fractionation, the absence of Eu* anomalies, high Sr/Y ratio, remarkably high $(Gd/Yb)_n$ values (>10), and the radiogenic Nd isotopic composition indicate that the dacitic melts were derived from a juvenile mafic source. According to petrogenetic estimations, such conditions could be caused by the partial melting of depleted N-MORB basites in equilibrium with an eclogitic residue. The dacitic magmas were likely generated by the partial melting of mafic rocks at lower levels of the significantly thickened crust (>60 km) in relation to collision processes.

Keywords: Paleoproterozoic, Volga–Don orogen, dacites, mantle source

DOI: 10.1134/S0869591124020073

INTRODUCTION

Paleotectonic reconstructions are one of the most important avenues of studying the evolution of the Earth's crust. Such reconstructions are conventionally carried out with the use of extensive information on magmatic complexes, because characteristics of their sources and parameters under which their melts were derived may serve as informative indicators of the tectonic settings. This approach plays a determining role in studying Early Precambrian complexes, in which many features of rocks needed for tectonic reconstructions have been obliterated by later processes (e.g., Moyen and Laurent, 2018).

In this paper, we utilize recently acquired data on the petrology of magmatic rocks to discuss reconstructions of the conditions and circumstances under which the Paleoproterozoic Vorontsovka terrane was formed. This terrane extends over a vast area between the ancient Sarmatia and Volga–Ural cratons and plays a pivoting role for understanding the crustal evolution of the East European craton during the Rhyasian–Orosirian period. A key point for understanding the mechanisms of crustal growth at that time is the powerful pulse of magmatism at 2050–2090 Ma, which produced numerous mafic–ultramafic, diorite, and granitoid plutons. The isotope age and geochemical characteristics of intrusions in the Vorontsovka terrane were viewed as evidence that they were formed in a postcollisional setting (Savko et al., 2014; Savko and Terentiev, 2017; Terentiev and Savko, 2016; Terentiev et al., 2016, 2018).

Quite recently, we have found subvolcanic bodies of sodic dacite porphyry depleted in HREE, LILE, and HFSE in the western margin of the Vorontsovka terrane. These features make the rocks similar to Archean high-pressure TTG associations and modern adakites and may be used as indicators of tectonic processes in the lithosphere of the Vorontsovka terrane.

Our study was centered on determining the U–Pb zircon age of the dacitic porphyries, identifying the sources of their melts based on the elemental and isotope geochemistry of the rocks, and understanding the tectonic setting in which the felsic magmatism developed.

GEOLOGY

The Volga–Don orogen is an extensive Paleoproterozoic subductional–collisional area between the Archean cores of the Sarmatia and Volga–Ural cratons (Fig. 1). It includes the Losevo and Don terranes, which are adjacent to the Kursk block, the extensive Vorontsovka terrane, and the Tersinskii belt, which is bounded by Archean Volga–Ural complexes in the east.

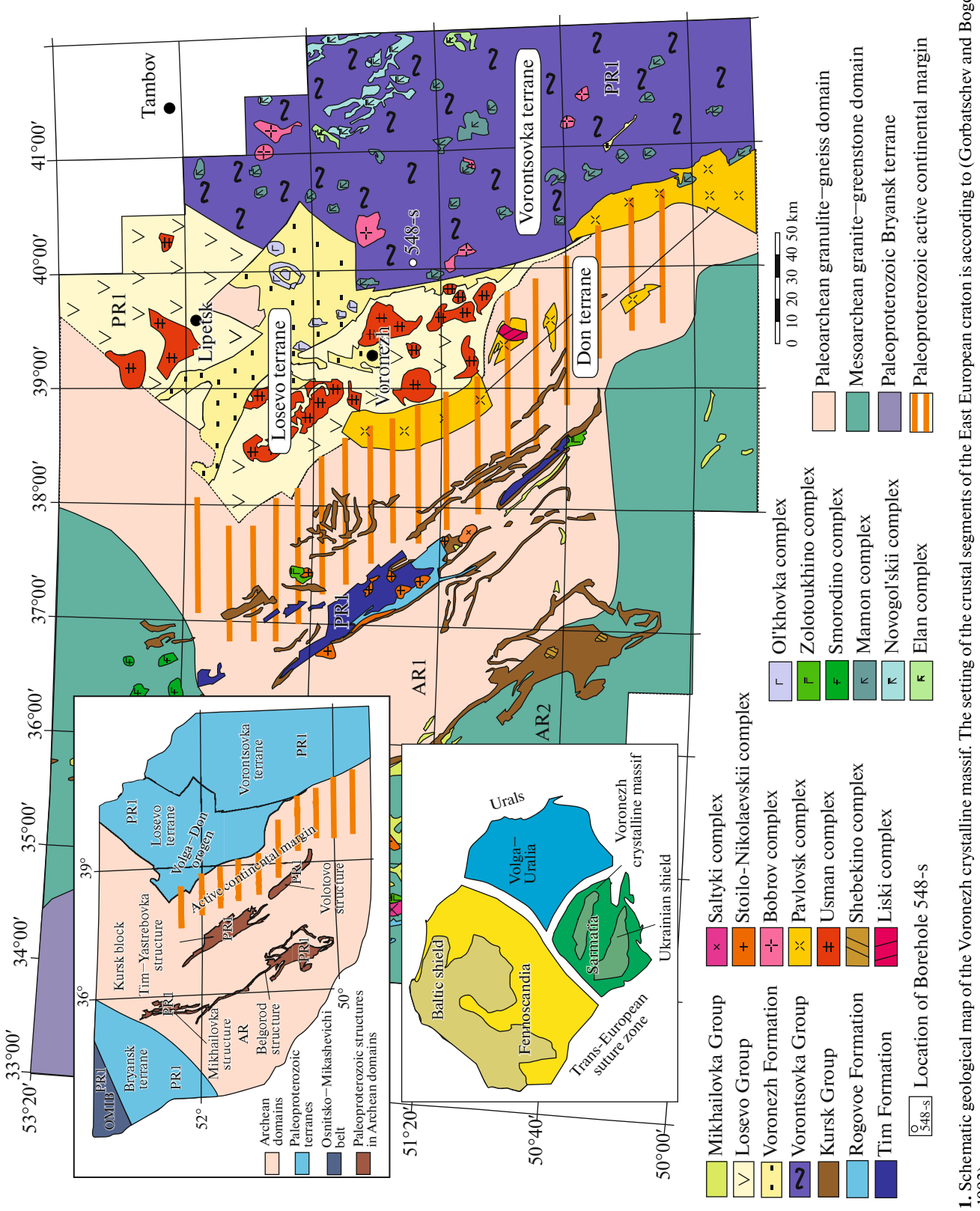

Fig. 1. Schematic geological map of the Voronezh crystalline massif. The setting of the crustal segments of the East European craton is according to (Gorbatschev and Bogdanova, 1993).

The Vorontsovka terrane is made up of folded metamorphosed Paleoproterozoic graywackes of the Vorontsovka Group 6–8 km thick (according to geophysical data). It extends for a distance over 600 km at a width of 100–300 km (Fig. 1). In the west, the terrane is bounded by the Losevo–Mamon deep fault, which separates this terrane from the Losevo and Don ones. In the south, it is terminated by the buried structures of the Azov block. In the east, the Vorontsovka terrane is bounded by the Paleoproterozoic Tersinskii belt of metavolcanic rocks and the South Volga supracrustal complex (Bibikova et al., 2009; Bogdanova et al., 2006).

The Vorontsovka terrane consists of a thick flyschoid sequence, which was accumulated in a tectonically active setting with weak chemical weathering of the rocks of different composition, from felsic to mafic (Savko et al., 2011). The sources of the terrigenous material were juvenile Paleoproterozoic arc complexes, as follows from Sm–Nd isotope data [$T_{Nd}(DM)$) of 2100 to 2400 Ma (Shchipansky et al., 2007)] and from the age of the detrital zircon of 2100–2200 Ma (Terentiev and Santosh, 2016). The metasedimentary rocks were affected by zoned HT/LP metamorphism at 3–5 kbar and 450–700°C (Savko, 1990, 1994) and were transformed into schists, metasandstones and into garnet–cordierite gneisses in high-temperature zones (Gerasimov and Savko, 1995). The metamorphic processes were dated at about 2069 Ma (Savko et al., 2015).

The metasedimentary sequences of the Vorontsovka terrane are cut by mafic intrusions and bodies of geochemically contrasting S- and A-type granites, which were dated at 2.05–2.07 Ga and have juvenile isotope signatures [$\varepsilon_{Nd}(T) = +2.0$ to $+2.6$)] (Savko et al., 2014). The S-type granites are believed to be produced by melting metasediments of the Vorontsovka Group in the marginal part of the terrane. The A_2 granites in the axial portion of the terrane were derived when the crustal thickness decreased. The A_2-type granites are differentiation products of mafic magmas emplaced into the lower crust and extensively contaminated with crustal material. The melts were emplaced after collision-related metamorphism at 2.07 Ga (Savko et al., 2014, 2015) in relation to postcollisional tectonics. The later platform magmatism produced gabbro-dolerites of the trap association of the Novogol'skii complex (Savko and Bocharov, 1988), dated at 1805 ± 14 Ma (Chernyshov et al., 2001), and Cambrian syenite dikes of the Artyushki complex (Nosova et al., 2019; Skryabin et al., 2015).

The Vorontsovka terrane is separated from the Kursk block by the Don terrane in the south and Losevo terrane in the north. The latter consists of island-arc edifices on an active continental margin, which are made up mostly of volcanics of a bimodal series dated at 2170–2120 Ma (Terentiev et al., 2017). These rocks were later intruded by large batholiths of I-type granites of the Usman complex, dated at 2100–2075 Ma, in a postcollisional environment, after a collisional event at approximately 2100 Ma (Terentiev et al., 2016; Shchipanskii et al., 2007).

The Don terrane is dominated by batholiths of I-type granitoids of the Pavlovsk complex, which were dated at 2081–2063 Ma (Terentiev et al., 2020) and abound in amphibolite xenoliths as large as a few meters, whose protoliths were mafic rocks of the Losevso Group. The protoliths of the Pavlovsk granitoids already contained an Archean crustal component. Toward the Archean Kursk block, they have progressively less radiogenic Nd isotopic composition, $\varepsilon_{Nd}(T)$ of +0.3 to −4.2, and xenogenic 2.8-Ga zircon appears in them (Terentiev et al., 2020).

The dacite porphyries were recovered by Borehole 548-s in the western part of the Vorontsovka terrane, not far from the boundary with the Losevo terrane (Figs. 1, 2). They occur as an array of nearly vertical (5°–7° to the borehole core axis) subvolcanic bodies (dikes) hosted in metapelite schists and metasandstones of the Vorontsovka Group, which are conformable with the foliation of the host rocks. The apparent thicknesses of the dacite bodies (as seen in the core material) range from 0.8 to 14.5 m (Fig. 2). With increasing depth, the orientation of the foliation and contacts with the dacites becomes more gently sloping, 40°–45° to the core axis. The dacites and their host metaterrigenous rocks were metamorphosed and show schistose structures, with the foliation conformable to that of the host schists and metasandstones. The rocks are cut across by relatively thin (no thicker than 1 cm) quartz and quartz–carbonate veinlets, some of which are conformable with the foliations and others cut it.

ANALYTICAL TECHNIQUES

Analysis for major oxides. Rocks were analyzed for major components by XRF on a S8 Tiger spectrometer (Bruker AXS GmbH, Germany) at the Voronezh State University (VSU). The procedure of sample preparation to analysis involved fusing 0.5 g of the powdered sample material with 2 g Li tetraborate in a muffle and subsequent casting of the glassy pellet. The spectrometer was calibrated and the quality of the analyses was controlled using state-certified reference samples for the chemical composition of rocks (GSO №8871-2007, GSO № 3333-85, GSO № 3191-85). The analyses were accurate to 1–5 relative % for components whose concentrations were higher than 1–5 wt % and up to 12 relative % at concentrations below 0.5 wt %. The raw analytical data were processed by conventional techniques implemented in the Spectra Plus software (Bruker AXS GmbH, Germany).

Analysis for trace elements and REE. Trace elements and REE were analyzed by ICP-MS at the Analytical

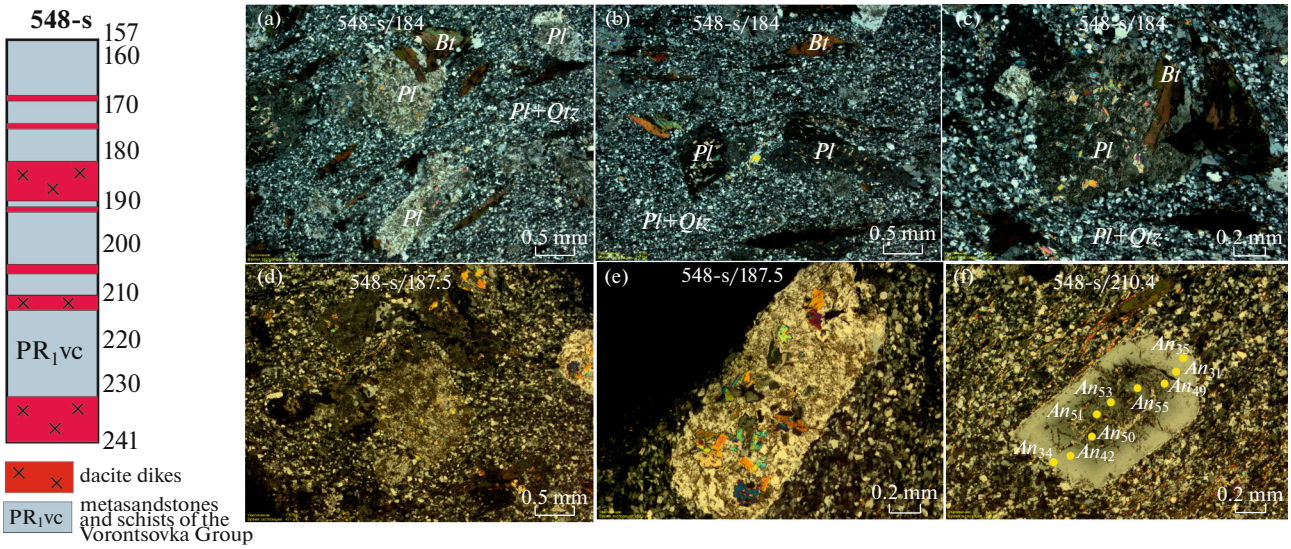

Fig. 2. Geological section through Borehole 548-s and microphotographs of thin sections of the dacite porphyries: (a–e) altered plagioclase xenocrysts in fine-grained quartz–feldspathic matrix; (f) zoning of a plagioclase xenocryst in dacite. Sample numbers in this figure: borehole number/depth.

Certification Testing Center of the Institute of the Technological Problems of Microelectronics and Ultrapure Materials in Chernogolovka in the Moscow area. The rock samples were decomposed by acids in open and closed systems depending on the composition of the rocks. The detection limits were 0.02–0.03 ppm for REE, Hf, Ta, Th, and U; 0.03–0.05 ppm for Nb, Be, and Co; 0.1 ppm for Li, Ni, Ga, and Y; 0.2 ppm for Zr; 0.3 ppm for Rb, Sr, and Ba; and 1–2 ppm for Cu, Zn, V, and Cr. The accuracy of the analysis was controlled by replicate analysis of the internationally and nationally certified standards GSP-2, VN, SGD-1A, and ST-1. Most elements were analyzed accurate to 3 to 5%.

The *isotope age of zircon* was measured on a SHRIMP-II ion probe at the Center for Isotope Studies of the Karpinsky Russian Geological Research Institute (VSEGEI) in St. Petersburg by the conventional technique (Larionov et al., 2004; Williams, 1998), using the 91500 and Temora zircon standards. The calculations were done using the decay constants from (Steiger and Jäger, 1977), with corrections for radiogenic Pb according to (Stacey and Kramers, 1975) on the basis of measured $^{204}Pb/^{206}Pb$. The results were processed with the SQUID v. 1.12 and ISOPLOT/Ex 3.22 software (Ludwig, 2005). Inasmuch as the results defined a discordia with a zero lower intercept, the age was evaluated by the upper intercept with the concordia. Following (Ludwig, 1998), concordance was understood as the fact that the concordia is overlapped by the 2σ error ellipse.

Sm–Nd whole-rock age. The Sm–Nd isotope studies were carried out at TsII VSEGEI. The Sm and Nd isotopic compositions were determined on a TRITON multicollector mass spectrometer in static mode. The measured $^{143}Nd/^{144}Nd$ ratios were normalized to $^{146}Nd/^{144}Nd = 0.7219$ and to $^{143}Nd/^{144}Nd = 0.512115$ in the JNdi-1 Nd standard. The Sm and Nd concentrations were measured accurate to ±0.5%, and the $^{147}Sm/^{144}Nd$ ± 0.5% and $^{143}Nd/^{144}Nd$ isotope ratios were determined accurate to ±0.005% (2σ).

Microprobe analysis (EPMA). Spot analyses of minerals were conducted on a Jeol 6380LV microprobe equipped with an Inca EDS system for quantitative analysis at VSU. Analyses were done at an accelerating voltage of 20 kV, beam current of 1.2 mA, counting time of 90 s, and a beam diameter of 1–3 μm. ZAF corrections were introduced when oxide concentrations were calculated and the accuracy was assessed using the proprietary software of the microprobe. The accuracy of the analysis was controlled on a systematic basis by replicate analysis of reference samples of natural and synthetic minerals.

PETROGRAPHY AND MINERALOGY

The dacites are pale gray to pale brownish gray schistose blastoporphyric rocks consisting of a fine-grained groundmass and feldspar phenocrysts, which make up to 30% of the rock by volume (Fig. 2). The matrix is lepidogranoblastic.

The dacites are dominated by plagioclase (60–80 mod. %), which occurs in the matrix and as phenocrysts up to 2–5 mm across and is often replaced by secondary fine-grained muscovite aggregates. Plagioclase in the fine-grained rock groundmass is oligoclase ($An_{10–23}$). The unaltered xenocrysts are concentrically zoned and have darker cores. The cores are more calcic ($An_{49–55}$) than the margins ($An_{31–35}$) (Fig. 2f). The

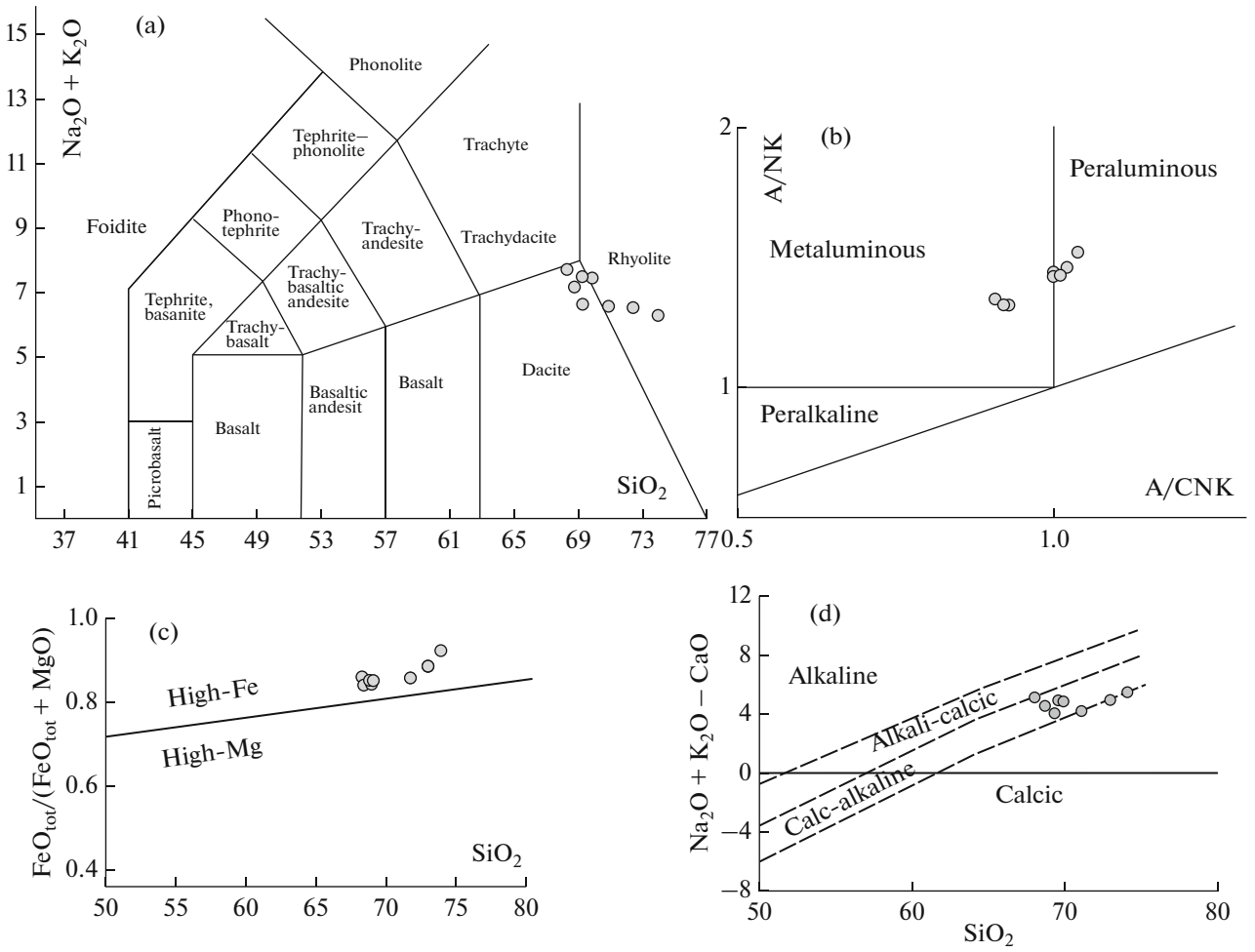

Fig. 3. Classification diagrams for the dacites of the Vorontsovka terrane: (a) $(Na_2O + K_2O)–SiO_2$; (b) A/CNK–A/NK; (c) $FeO_{tot}/(FeO_{tot} + MgO)–SiO_2$; (d) $(Na_2O + K_2O - CaO)–SiO_2$.

groundmass contains minor amounts (no more than 5 mod. %) of potassic feldspar. The fine-grained matrix contains up to 20 modal % quartz.

Biotite (2–5 modal %) is the only mafic mineral and occurs as elongate brown laths up to 2 mm long, is Fe-rich (X_{Fe} = 0.72–0.81), and contains much TiO_2 (2.4–2.9 wt %). The accessory minerals are apatite, titanite, and zircon, the ore minerals are magnetite and sphalerite, and the secondary ones are chlorite, epidote, and calcite.

GEOCHEMISTRY

The dacites contain 67.9 to 74.4 wt % SiO_2, intermediate concentrations of alkalis ($Na_2O + K_2O$ = 6.3–7.8 wt %), with Na obviously dominating over K (K_2O/Na_2O = 0.44–0.77), intermediate concentrations of TiO_2 (0.1–0.4 wt %), and have X_{Fe} = 0.69–0.84 and A/CNK close to 1.0 (Fig. 3, Table 1). In the TAS classification diagram (Middlemost, 1994), the composition points of the rocks plot within the fields of dacites and rhyolites (Fig. 3). Binary diagrams show negative correlations of SiO_2 with TiO_2, CaO, Al_2O_3, MgO, and K_2O (Fig. 4).

The dacites are typically low in such "mafic elements" as Ni and Cr and in all HFSE (particularly Y) but are high in Sr (Sr/Y = 83–150), and contain moderate concentrations of Ba and Rb (Table 1). The rocks are also depleted in REE, whose normalized patterns are negatively sloped, with enrichment in LREE and with their very significant fractionation [$(La/Yb)_n$ = 56–177] and without clearly discernible Eu* anomaly (Table 1, Fig. 5), with very high $(Gd/Yb)_n$ = 10–19. The normalized multielemental patterns of the rocks show negative Nb and weak positive Ti anomalies (Fig. 5).

U–Pb ZIRCON GEOCHRONOLOGY

Zircon from a metadacite dike, sample 548-s/185.7 (Borehole 548-c, depth 185.7 m) was dated based on SHRIMP-II analyses. The zircon forms colorless

Table 1. Concentrations of major oxides, trace elements, and REE in the dacites of the Vorontsovka terrane

Component	548-s/ 184.5*	548-s/ 185.7	548-s/ 186	548-s/ 187	548-s/ 187.5	548-s/ 190	548-s/ 210.4	548-s/ 237.6
SiO_2	69.43	68.49	69.01	69.63	67.93	71.08	72.44	74.36
TiO_2	0.34	0.38	0.40	0.36	0.41	0.36	0.23	0.07
Al_2O_3	14.82	15.48	14.93	14.83	15.11	14.25	14.31	14.40
Fe_2O_{3tot}	3.22	3.65	3.68	2.97	3.69	3.17	2.68	1.83
MgO	0.70	0.84	0.81	0.67	0.73	0.70	0.42	0.18
MnO	0.03	0.02	0.02	0.03	0.04	0.04	0.03	0.02
CaO	2.90	2.99	2.80	3.09	3.06	2.71	2.53	1.88
Na_2O	4.70	4.21	3.98	4.34	4.40	3.90	4.41	4.39
K_2O	2.75	2.92	2.80	3.18	3.40	2.72	2.13	1.91
P_2O_5	0.18	0.17	0.17	0.17	0.22	0.19	0.10	0.04
SO_3	0.04	0.10	0.15	0.12	0.06	0.05	0.04	0.06
LOI.	0.66	0.62	1.11	0.55	0.89	0.67	0.62	0.70
Total	99.77	99.82	99.76	99.93	99.93	99.92	99.94	99.83
X_{Mg}	0.30	0.31	0.30	0.31	0.28	0.30	0.34	0.16
K_2O/Na_2O	0.59	0.69	0.70	0.73	0.77	0.70	0.48	0.44
$Na_2O + K_2O$	7.45	7.13	6.78	7.52	7.80	6.62	6.54	6.30
A/CNK	0.93	1.00	1.02	0.91	0.92	1.00	1.01	1.13
Li	23	26.3			26	11	6	5.0
Be	1.9	1.3			1.6	0.9	0.9	1.7
Sc	2.2	1.6			2.1	2.1	0.6	1.3
V	22	21.4			15	8	6	15.4
Cr	22	24.3			14	7	8	20.2
Co	4	3.4			3	1.6	0.9	0.77
Ni	5	2.1			4	1.4	1.5	3.3
Ga	26	21.9			24	12	10	17.8
Rb	30	59.9			40	6	6	32.4
Sr	300	506			300	80	50	322
Y	2	3.7			2	0.8	0.6	2.3
Zr	170	160			160	85	58	61.1
Nb	8	8.0			8	3.8	3.9	7.8
Mo	1.1	1.2			0.9	1.8	0.6	0.57
Cs	1.1	2.2			1.4	0.7	0.5	0.67
Ba	380	713			400	180	150	611
La	9	28.0			10	3.1	3	20.5
Ce	22	59.3			23	7	7	42.0
Pr	2.9	6.8			3.1	1	0.9	4.4
Nd	11	26.8			12	4.1	3.6	17.6
Sm	1.9	4.4			2.1	0.7	0.6	3.5
Eu	0.6	1.0			0.7	0.23	0.18	0.69
Gd	1.3	2.4			1.4	0.49	0.42	1.9
Tb	0.09	0.22			0.1	0.04	0.03	0.19
Dy	0.42	0.93			0.45	0.18	0.15	0.63
Ho	0.06	0.12			0.06	0.025	0.02	0.072

Table 1. (Contd.)

Component	548-s/ 184.5*	548-s/ 185.7	548-s/ 186	548-s/ 187	548-s/ 187.5	548-s/ 190	548-s/ 210.4	548-s/ 237.6
Er	0.16	0.25			0.11	0.052	0.039	0.12
Tm	0.015	0.029			0.015	0.007	0.005	0.011
Yb	0.09	0.19			0.09	0.04	0.03	0.083
Lu	0.012	0.024			0.012	0.006	0.004	0.010
Hf	3	4.3			2.9	1.8	1.5	2.3
Ta	0.46	0.71			0.5	0.28	0.33	0.67
W	0.18	1.3			0.16	0.3	0.11	1.1
Pb	7	12.7			7	5	6	15.6
Th	2.8	5.1			2.7	1.1	1	4.6
U	1.4	1.7			1.3	0.7	1	2.2
∑REE	49.6	131			53.1	17.0	16.0	91.8
Eu/Eu*	1.17	0.94			1.25	1.20	1.10	0.82
$(Gd/Yb)_n$	12.0	10.5			12.9	10.1	11.6	18.9
$(La/Yb)_n$	71.7	106			79.7	55.6	71.7	177.2
Sr/Y	150	137			150	100	83.3	140
Yb_n	0.53	1.12			0.53	0.24	0.18	0.49

* Borehole/depth.

euhedral and subhedral prismatic crystals, with numerous long-prismatic grains (150–200 μm long) that have acute pyramidal termination (Fig. 6). The crystals sometimes contain solid inclusions. The CL images of these crystals display their growth structures: thin concentric oscillatory zoning. No clearly seen inherited cores of the grains were found. Structural and morphological features of these grains suggest their magmatic nature and the almost absolute absence of any overprinted transformations.

We conducted 16 spot analyses of 15 grains (Table 2, Fig. 7). In a concordia plot, all data are approximated by a single regression line with closely similar concordant age values. No appreciable differences were found between the inner and outer portions of the crystals. The upper intercept of the regression line with the concordia for all analytical spots corresponds to an age of 2069 ± 20 Ma (N = 16, MSWD = 0.42). The concordant age (N = 12) is 2069 ± 13 Ma (MSWD = 0.0052, concordance probability = 0.94) (Fig. 7).

Sm–Nd ISOTOPE DATE

The isotope composition of Nd was analyzed in two whole-rock samples of the dacite: 548-s/185.7, whose zircon isotope age has been determined, and 548-s/237.6. The $\varepsilon_{Nd}(2069)$ = 2.6 and 3.4, and the model age $T_{Nd}(DM)$ is 2258 and 2222 Ma (Table 3, Fig. 8), respectively, which indicates that the crustal prehistory of the juvenile mantle sources of the melts was brief.

GEOCHEMICAL TYPES

According to their geochemical features, the dacites of the Vorontsovka terrane are iron-rich, mostly metaluminous rocks of the calc-alkaline series. In spite of their high Fe#, these rocks cannot be classed with A-type granites, which are characterized by potassic alkalinity, are typically enriched in HFSE and REE, and have negative Eu* anomalies. The relatively low Al# of the rocks and the fact that they do not contain muscovite (and/or garnet, cordierite), low LILE concentrations, and predominantly sodic alkalinity make the dacites different from S-type granitoids. These rocks differ from M-type granitoids in having strongly fractionated LREE and HREE patterns. In discriminant diagrams in terms of "alphabetic" classification, the dacites fall within the fields of I-, S-, and M-type granites (Whalen et al., 1987), and they plot within the field of arc granites in the Rb vs. (Y + Nb) diagram (Pearce et al., 1984) (Fig. 9). It is thus reasonable to believe that the dacites of the Vorontsovka terrane are I-type granitoids.

According to their geochemical features, the dacites of the Vorontsovka terrane are close to high-pressure trondhjemites of Archean TTG associations (Moyen, 2011) (Fig. 10) but differ from them in being more strongly depleted in LILE and HFSE, having higher Fe#, and anomalously strongly fractionated LREE and HREE patterns. The dacites differ from typical adakites in containing low concentrations of the compatible elements Ni and Cr and those of Mg. In the latest geochemical review (Sotiriou et al., 2023),

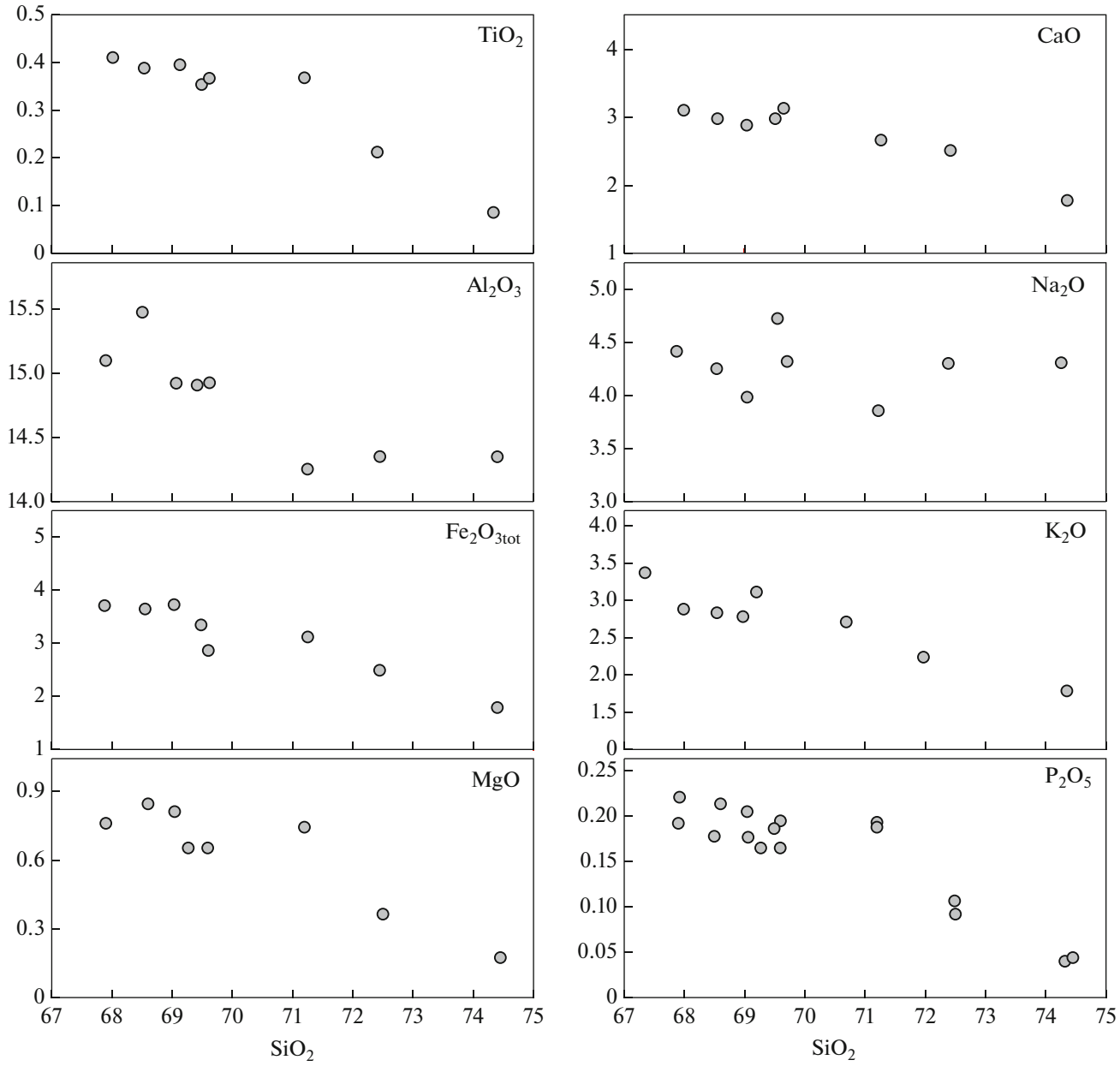

Fig. 4. Diagrams showing the distributions of major oxides.

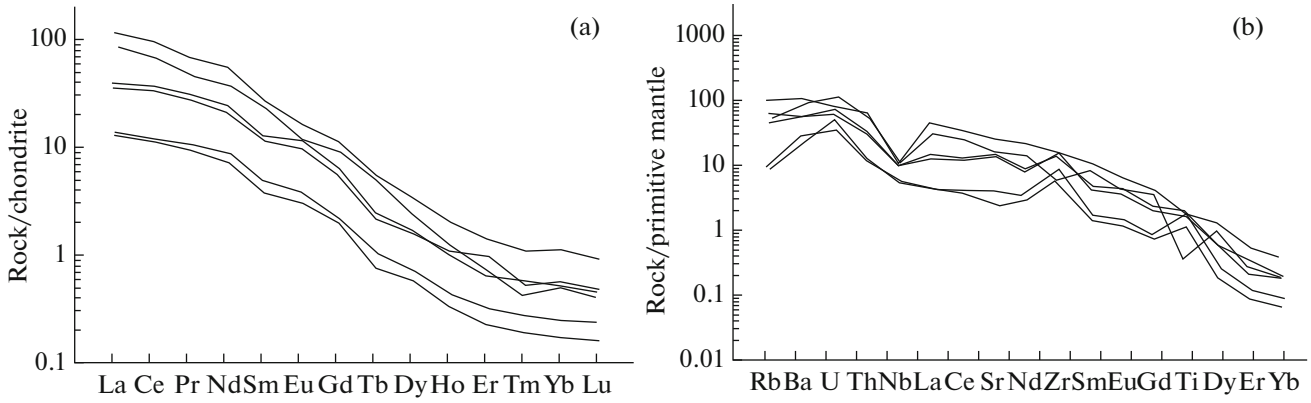

Fig. 5. (a) Chondrite- and (b) primitive mantle-normalized multielemental patterns.

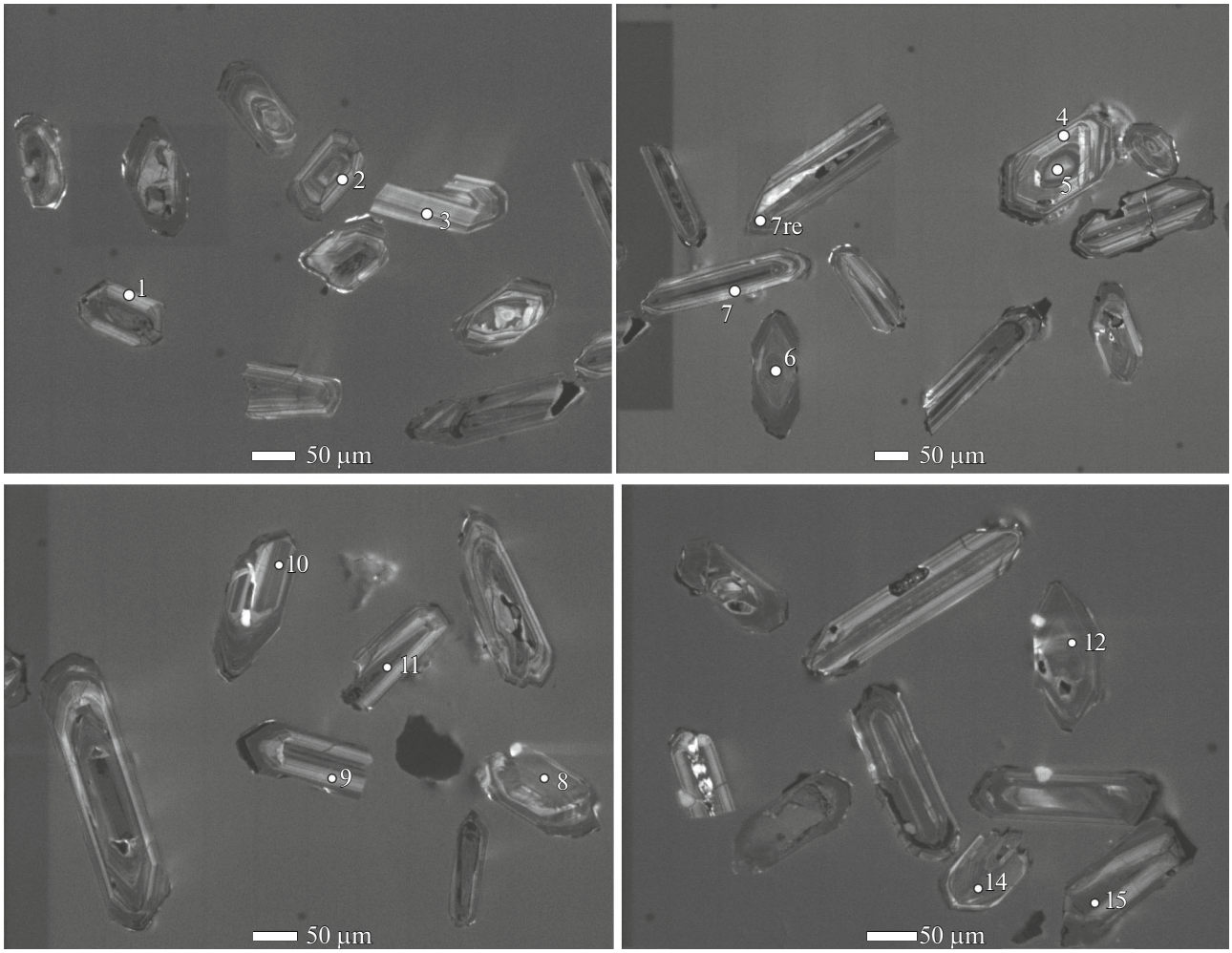

Fig. 6. CL images of zircon grains from the metadacites of the Vorontsovka terrane. Small white circles with numerals are the spots of SHRIMP-II analyses. The numbers of the analytical spots correspond to the numbers of analyses in Table 2.

Archean TTG associations with $(Gd/Yb)_n > 10$ are very sparse (a few instances). They are also very rare among Proterozoic and Phanerozoic trondhjemites and adakites.

PETROGENESIS

The strongly depleted HREE patterns of the rocks indicate that the dacite melts were derived by melting in equilibrium with a garnet-bearing residue. The sodic specifics of the rocks, their low concentrations of incompatible elements, and the high radiogenic Nd isotope composition provide grounds to think that the dacitic melts were derived from a depleted mafic source. Petrogenetic calculations indicate that this might have occurred at the partial melting of depleted mafic rocks of the N-MORB type in equilibrium with eclogitic residue (Fig. 11). This is consistent with experimental data, according to which dacitic melts can be derived via 20–40% melting of metabasalt at

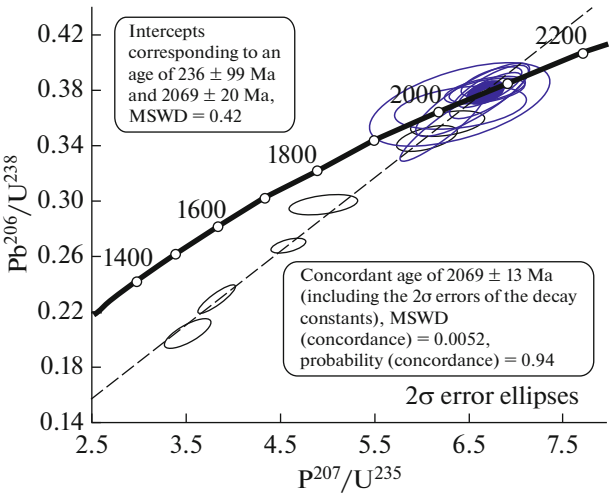

Fig. 7. U–Pb concordia plots for zircon from the metadacites of the Vorontsovka terrane: SIMS data.

Table 2. U–Pb geochronologic data (SHRIMP-II) on zircon from the metadacites

Spot	$^{206}Pb_c$, %	U, ppm	Th, ppm	$^{206}Pb^*$, ppm	$^{232}Th/^{238}U$	(1) $^{206}Pb/^{238}U$	±Ma	(1) $^{207}Pb/^{206}Pb$	±Ma	*D*, %	(1) $^{238}U/^{206}Pb^*$	±%	(1) $^{207}Pb^*/^{206}Pb^*$	±%	(1) $^{207}Pb^*/^{235}U$	±%	(1) $^{206}Pb^*/^{238}U$	±%	Corr. err.
Sample 548-c/185.7																			
7	4.22	762	540	150	0.73	1330	21	1972	20	+36	4.4	1.8	0.121	1.1	3.8	2.1	0.23	1.8	0.8
4	2.85	290	58	73.9	0.21	1677	16	1975	51	+17	3.4	1.1	0.121	2.8	5.0	3.0	0.30	1.1	0.4
1	3.64	661	92	152	0.14	1530	12	2015	24	+27	3.7	0.9	0.124	1.4	4.6	1.6	0.27	0.9	0.5
9	5.33	476	117	83.7	0.25	1199	23	2022	34	+45	4.9	2.1	0.125	1.9	3.5	2.8	0.20	2.1	0.7
2	1.56	367	86	109	0.24	1911	18	2061	32	+8	2.9	1.1	0.127	1.8	6.1	2.1	0.35	1.1	0.5
7re	1.40	486	130	147	0.28	1945	45	2073	22	+7	2.8	2.7	0.128	1.3	6.2	3.0	0.35	2.7	0.9
11	1.42	261	48	79.8	0.19	1961	18	2073	42	+6	2.8	1.1	0.128	2.4	6.3	2.6	0.36	1.1	0.4
3	1.07	155	22	48.9	0.15	2015	30	2058	73	+2	2.7	1.7	0.127	4.1	6.4	4.5	0.37	1.7	0.4
5	1.06	111	31	35.3	0.29	2029	58	2040	90	+1	2.7	3.3	0.126	5.1	6.4	6.1	0.37	3.3	0.6
10	0.69	241	79	77.1	0.34	2037	49	2055	38	+1	2.7	2.8	0.127	2.1	6.5	3.5	0.37	2.8	0.8
3	0.34	314	52	102	0.17	2072	20	2066	41	0	2.6	1.1	0.128	2.3	6.7	2.6	0.38	1.1	0.4
8	0.23	226	46	73.7	0.21	2077	20	2070	39	0	2.6	1.1	0.128	2.2	6.7	2.5	0.38	1.1	0.4
12	0.15	438	89	143	0.21	2077	32	2074	29	0	2.6	1.8	0.128	1.7	6.7	2.5	0.38	1.8	0.7
15	0.16	561	55	184	0.10	2081	26	2075	26	0	2.6	1.5	0.128	1.5	6.7	2.1	0.38	1.5	0.7
6	0.38	467	136	152	0.30	2074	37	2078	26	0	2.6	2.1	0.129	1.5	6.7	2.6	0.38	2.1	0.8
14	0.00	452	109	149	0.25	2097	17	2060	29	–2	2.6	1.0	0.127	1.7	6.7	1.9	0.38	1.0	0.5

The errors are 1σ; Pb_c and Pb* are common and radiogenic Pb, respectively. The standard calibration error is 0.3%. (1) Common Pb corrected by the measured ^{204}Pb. *D*, % is the discordance in %.

Table 3. Sm–Nd isotope data on the dacite porphyries

Sample	Sm, ppm	Nd, ppm	$^{147}Sm/^{144}Nd$*	$^{143}Nd/^{144}Nd$	T**, Ma	$\varepsilon_{Nd}(T)$	$T_{Nd}(DM)$***
548-s/185.7	4.18	27.05	0.0935	0.511364	2069	2.6	2258
548-s/237.6	3.56	20.24	0.10644	0.511582	2069	3.4	2222

* The error in $^{147}Sm/^{144}Nd$ was assumed to be no higher than 0.2%. ** Age according to U–Pb dating (see text). *** Model age according to (Goldstein and Jacobsen, 1988).

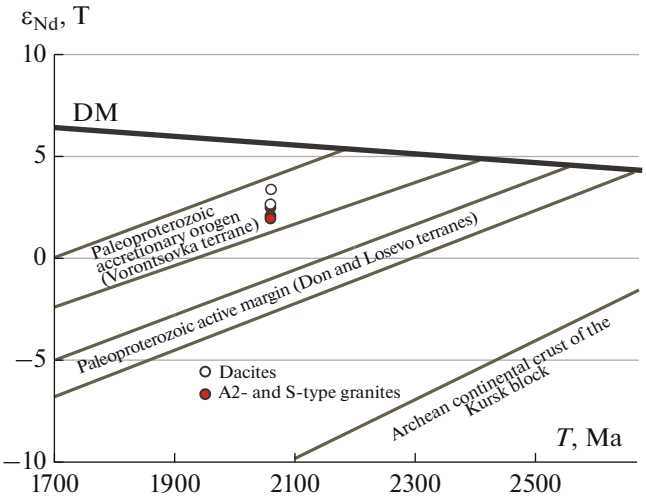

Fig. 8. Results of Sm–Nd study of the metadacites from the Vorontsovka terrane. Data on the granites of the Vorontsovka terrane are from (Savko et al., 2014).

1000–1100°C and 16–32 kbar in equilibrium with eclogite residue (Hastie et al., 2016; Rapp and Watson, 1995).

Changes in the composition of dacite toward rhyolite composition may be explained by crystallization differentiation. The major cumulus phase was likely plagioclase, whose phenocrysts are widespread in these rocks (Fig. 2) and were likely entrained from an intermediate chamber. The massive crystallization of plagioclase may have been triggered by a pressure decrease during the ascent of the felsic magmas and resulted in noticeable decrease in concentrations of Al_2O_3, CaO, Sr, and Eu in the rhyolites. The radical decrease in the concentrations of all REE with the transition from the dacites to rhyolites may have been caused by the crystallization of a calcic accessory mineral that could concentrate REE, for example, titanite and/or apatite (Fig. 10).

The geochemical and isotope features of the dacite suggest that they could be generated by the melting of

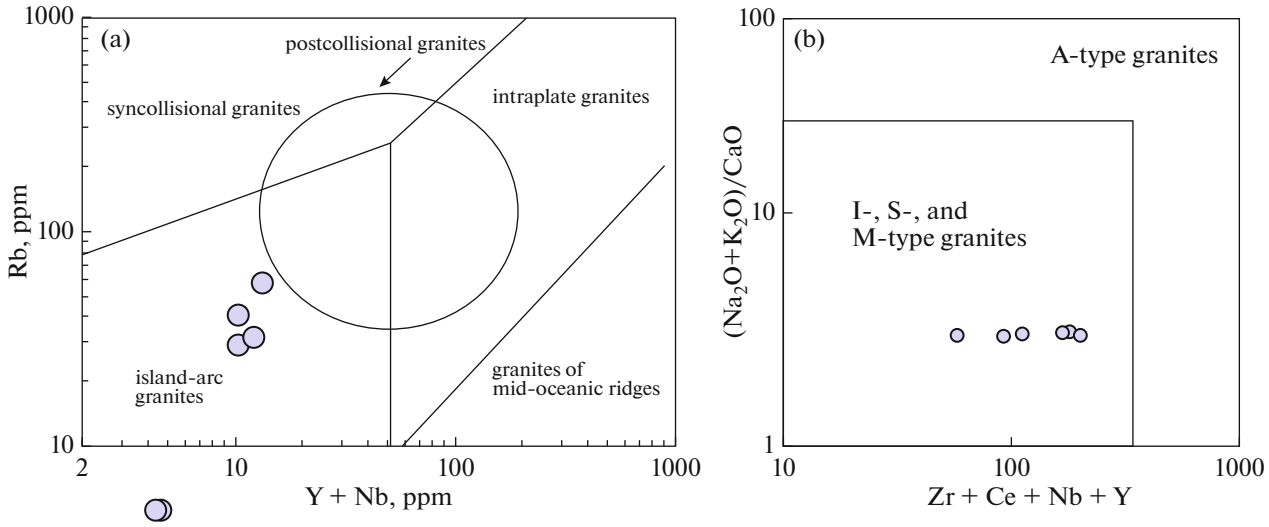

Fig. 9. Discriminant diagrams for the metadacites of the Vorontsovka terrane: (a) according to (Pearce, 1996); (b) according to (Whalen et al., 1987).

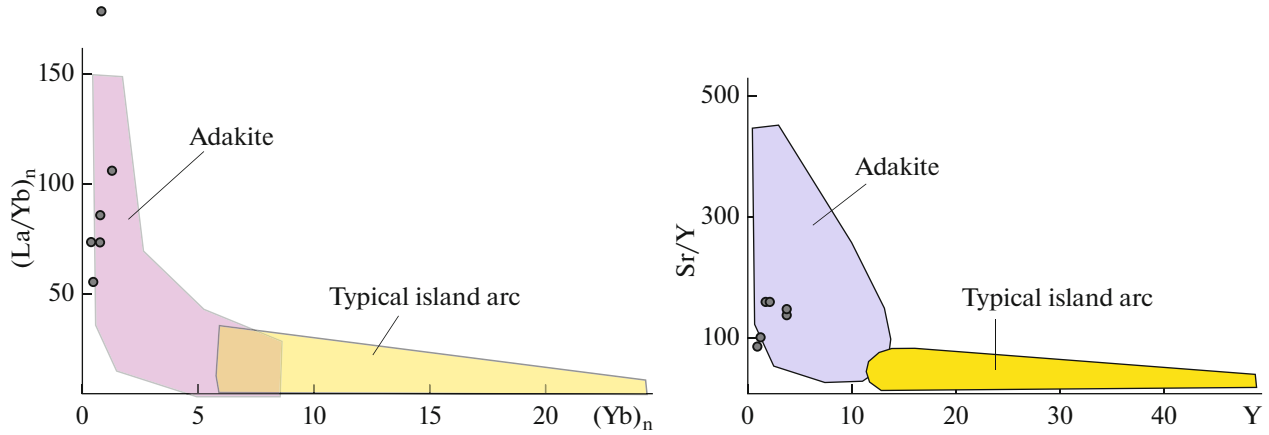

Fig. 10. Discriminant diagrams (Drummond and Defant, 1990) for the dacites of the Vorontsovka terrane.

a depleted mafic sources of the N-MORB type at depths greater than 60 km, in equilibrium with an eclogite residue, and subsequent differentiation at shallow depths. This petrogenetic scenario might have been implemented in a subduction zone at the melting of a down-going oceanic slab (Martin and Moyen, 2002). However, this scenario is inconsistent with the low Mg# of the dacites and their low MgO, Cr, and Ni concentrations, which rules out that the felsic subductional melts could interact with rocks of the overlying mantle wedge (Martin, 1999; Smithies, 2000). Melts of such composition could be derived in tectonic settings of the following two types: (1) low-angle subduction and (2) crustal thickening at collision that had occurred before the dacites were derived.

In the situation of low-angle subduction, such magmas could be brought to the lower crust without any significant changes in their composition (Martin and Moyen, 2002). For example, derivatives of slab melting (adakite magmas in the Japanese island arc) retain low MgO, Cr, and Ni concentrations (Tsuchiya et al., 2007).

A likely more probable scenario is that the dacitic magmas were derived by the melting of the lower levels of strongly thickened mafic crust. Its thickening (the formation of an orogenic wedge) occurred before the 2.069-Ga dacite dikes were emplaced as a result of collisional processes during subduction (arc–continent collision), likely at about 2.1 Ga (Tsybulyaev et al., 2021; Korish et al., 2022). Collision and associated metamorphism reoccurred (or continued) at the collision of Sarmatia and Volga–Uralia (continent–continent collision) at about 2.07 Ga (Savko et al., 2015, 2018).

It has been demonstrated that the collision and metamorphism proceeded when the lithosphere of the young Vorontsovka terrane was “warm” and “wet”

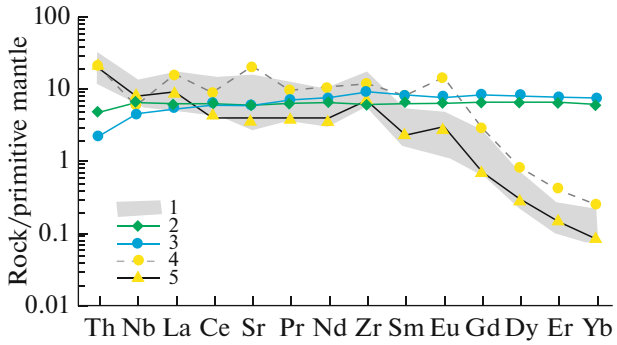

Fig. 11. Results of numerical simulations of the origin of the dacites and rhyolites. (1) Composition field of the natural rock samples; (2, 3) hypothetical sources of the melts: (2) MORB-type tholeiite from the bottom portion of the Losevo Group (sample 7782/422 from Shchipansky et al., 2007); (3) average N-MORB (White and Klein, 2014); (4) model dacitic melt produced by 20% equilibrium melting of tholeiite, with the residue consisting of clinopyroxene (50%), garnet (48%), and rutile (2%); (5) model rhyolitic melt produced by 30% differentiation of dacitic melt with the removal of the cumulus association of plagioclase plagioclase (90%) + apatite (9%) + zircon (1%). The calculations were carried out using formulas in (Arth, 1976) and partition coefficients in (Rollinson and Pease, 2021).

(Savko et al., 2015), and this was favorable for the eclogitization of the lower crustal mafic rocks. The partial melting of the eclogite protoliths was triggered by fluids that were released in the course of metamorphic reactions of dehydration and/or at delamination in the bottom part of the crust and magmatic underplating.

Scenarios of this type for the derivation of adakite magmas at the melting of thickened mafic lower crust were proposed for the Early Paleozoic collisional orogen Qinling in southern China (Qin et al., 2015) and the Miocene Himalayan–Tibetan collisional orogen (Chung et al., 2003; Hou et al, 2004; Wang et al., 2005). Note that the Volga–Don collisional orogen is thought to be a Paleoproterozoic analogue of the Himalayan–Tibetan orogen (Shchipansky and Kheraskova, 2023).

CONCLUSIONS

Metamorphosed dacite porphyry dikes (crystallization age 2069 ± 13 Ma) were first found among metaterrigenous flyschoid sequences of the Vorontsovka Group in the western part of the Vorontsovka terrane, at its boundary with the Losevo terrane. These are iron-rich, mostly metaluminous rocks of the calc-alkaline series and correspond to I-type granites. Such geochemical features and sodic alkalinity, depletion in LILE, HFSE, compatible elements, and REE, with the strong fractionation of the latter, and the absence of an Eu* anomaly, high Sr/Y ratios, and particularly $(Gd/Yb)_n > 10$ and a radiogenic Nd isotope composition suggest that the melts were derived via the partial melting of juvenile mafic protoliths of the MORB type under high pressures, in equilibrium with garnet–pyroxene eclogitic residue. We believe that the dacites may have been formed either as a result of low-angle subduction of an oceanic slab beneath the Sarmatia craton or by the partial melting of highly thickened (>60 km) eclogitized mafic lower crust when the orogen was formed. The change in composition from dacite to rhyolite may have been caused by crystallization differentiation.

ACKNOWLEDGMENTS

The authors thank the reviewers A.A. Shchipansky (Geological Institute, Russian Academy of Sciences) and Yu.A. Martynov (Far East Geological Institute, Far East Branch, Russian Academy of Sciences) for attention to the manuscript and valuable comments, which led us to improve the manuscript.

FUNDING

This work was supported by ongoing institutional funding for IGEM RAS. No additional grants to carry out or direct this particular research were obtained.

CONFLICT OF INTEREST

The authors of this work declare that they have no conflicts of interest.

OPEN ACCESS

REFERENCES

Arth, J.G., Behavior of trace elements during magmatic processes—a summary of theoretical models and their applications, *J. Res. U.S. Geol. Surv.,* 1976, vol. 4, no. 1, pp. 41–47.

Bibikova, E.V., Bogdanova, S.V., Postnikov, A.V., et al., Sarmatia–Volgo-Uralia Junction Zone: Isotopic–Geochronologic Characteristic of Supracrustal Rocks and Granitoids, *Stratigraphy. Geol. Correlation,* 2009, vol. 17, no. 6, pp. 561–573.

Bogdanova, S., Gorbatschev, R., Grad, M., et al., EUROBRIDGE: new insight into the geodynamic evolution of the East European craton, European Lithosphere Dynamics, Gee, D.C. and Stephenson, R.A., Eds., *Geol. Soc. London: Mem.,* 2006, vol. 32, no. 1, pp. 599–625.

Chernyshov, N.M., Bayanova, T.B., Al'bekov, A.Yu., and Levkovich, N.V., New data on the age of gabbro–dolerite intrusions of the trap formation in the Khoper Megablock, Voronezh crystalline massif, Central Russia, *Dokl. Earth Sci.,* 2001, vol. 381, no. 8, pp. 889–891.

Chung, S.L., Liu, D., Ji, J., et al., Adakites from continental collision zones: melting of thickened lower crust beneath southern Tibet, *Geology,* 2003, vol. 31, pp. 1021–1024.

Drummond, M.S. and Defant, M.J., A model for trondhjemite–tonalite–dacite genesis and crustal growth via slab melting: Archean to modern comparisons, *J. Geophys. Res.,* 1990, vol. 95, pp. 21503–21521.

Gerasimov, V.Yu. and Savko, K.A., Geospidometry and temperature evolution of the garnet—cordierite metapelites of the Voronezh crystalline massif, *Petrology,* 1995, vol. 3, no. 6, pp. 511–524.

Goldstein, S.J. and Jacobsen, S.B., Nd and Sr isotopic systematics of river water suspended material: implications for crustal evolution, *Earth Planet. Sci. Lett.,* 1988, vol. 87, pp. 249–265.

Gorbatschev, R. and Bogdanova, S., Frontiers in the Baltic shield, *Precambrian Res.,* 1993, vol. 64, pp. 3–21.

Hastie, A.R., Fitton, J.G., Bromiley, G.D., et al., The origin of Earth's first continents and the onset of plate tectonics, *Geology,* 2016, vol. 44, pp. 855–858.

Hou, Z.Q., Gao, Y.F., Qu, X.M., et al., Origin of adakitic intrusives generated during Mid-Miocene east-west extension in southern Tibet, *Earth Planet. Sci. Lett.,* 2004, vol. 220, pp. 139–155.

Korish, E.Kh., Savko, K.A., Sal'nikova, E.B., et al., Paleoproterozoic diorite—granodiorite magmatism of the Kursk block, Sarmatia: deciphering the temporally close geological events, *Tr. Karel'skogo NTs RAN,* 2022, no. 5, pp. 60–63.

Larionov, A.N., Andreichev, V.A., and Gee, D.G., The Vendian alkaline igneous suite of northern Timan: ion microprobe U-Pb zircon ages of gabbros and syenite, *The Neoproterozoic Timanide Orogen of Eastern Baltica,* Gee, D.C. and Pease, V.L., Eds., *Geol. Soc. London Mem.,* 2004, vol. 30, no. 1, pp. 69–74.

Ludwig, K.R., On the treatment of concordant uranium-lead ages, *Geochim. Cosmochim. Acta,* 1988, vol. 62, pp. 665–676.

Ludwig, K.R., *User 's Manual for ISOPLOT/Ex 3.22. A Geochronological Toolkit for Microsoft Excel,* Berkeley Geochronol. Center, Sp. Publ, 2005. http://www. bgc.org/klprogrammenu.html.

Martin, H., The adakitic magmas: modern analogues of Archaean granitoids, *Lithos,* 1999, vol. 46, pp. 411–429.

Martin, H. and Moyen, J.-F., Secular changes in TTG composition as markers of the progressive cooling of the Earth, *Geology,* 2002, vol. 30, pp. 319–322.

Middlemost, E.A.K., Naming materials in the magma/igneous rock system, *Earth-Sci. Rev.,* 1994, vol. 37, p. 215.

Moyen, J.F., The composite Archaean grey gneisses: petrological significance, and evidence for a non-unique tectonic setting for Archaean crustal growth, *Lithos,* 2011, vol. 123, nos. 1–4, pp. 21–36.

Moyen, J.-F. and Laurent, O., Archaean tectonic systems: a view from igneous rocks, *Lithos,* 2018, vol. 302–303, pp. 99–125.

Nosova, A.A., Voznyak, A.A., Bogdanova, S.V., et al., Early Cambrian syenite and monzonite magmatism in the southeast of the East European Platform: petrogenesis and tectonic setting, *Petrology,* 2019, vol. 27, no. 4, pp. 329–369.

Pearce, J.A., Harris, N.W., and Tindle, A.G., Trace element discrimination diagrams for the tectonic interpretation of granitic rocks, *J. Petrol.,* 1984, vol. 25, pp. 956–983.

Pearce, J.A., *A user's guide to basalt discrimination diagrams, Trace Element Geochemistry of Volcanic Rocks: Applications for Massive Sulphide Exploration,* Wyman, D.A., Eds., *Geol. Ass. Can., Short Course Notes,* 1996, vol. 12, pp. 79–113.

Qin, Z., Wu, Y., Siebel, W., et al., Genesis of adakitic granitoids by partial melting of thickened lower crust and its implications for early crustal growth: a case study from the Huichizi pluton, Qinling orogen, central China, *Lithos,* 2015, vol. 238, pp. 1–12.

Rapp, R.P. and Watson, E.B., Dehydration melting of metabasalt at 8–32 kbar: implications for continental growth and crust–mantle recycling, *J. Petrol.,* 1995, vol. 36, pp. 891–931.

Rollinson, H. and Pease, V., *Using Geochemical Data to Understanding Geological Processes,* 2nd Ed., Cambridge: Cambridge University Press, 2021.

Savko, K.A., Zoning of minerals and prograde metamorphic reactions in the medium-temperature metapelites of the Vorontsovka Group (Voronezh Crystalline Massif), *Izv. Akad. Nauk SSSR. Ser. Geol.,* 1990, no. 11, pp. 79–87.

Savko, K.A., Low-temperature rocks in the metamorphic zoning of the Vorontsovka Group, VCM, *Geol. Geofiz.,* 1994, no. 3, pp. 50–59.

Savko, K.A. and Bocharov, V.L., Petrochemistry of gabbrodolerites of the eastern Voronezh crystalline massif, *Izv. Vyssh. Ucheb. Zaved, Geol. Razved.,* 1988, no. 7, pp. 42–51.

Savko, K.A. and Terentiev, R.A., Geochronology of the quartz diorites of theRomanovsky pluton, Voronezh crystalline massif, *Vestn. Voronezhsk. Univ., Ser. Geol.,* 2017, no. 2, pp. 74–80.

Savko, K.A., Samsonov, A.V., Bazikov, N.S., Metaterrigenous rocks of the Vorontsovka Group of the Voronezh crystalline massif: geochemistry, specifics of formation, and source areas, *Vestn. Voronezhsk. Univ., Ser. Geol.,* 2011, no. 1, pp. 70–94.

Savko, K.A., Samsonov, A.V., Larionov, A.N., et al., Paleoproterozoic A- and S-granites in the eastern Voronezh Crystalline Massif: geochronology, petrogenesis, and tectonic setting of origin, *Petrology,* 2014, vol. 22, no. 3, pp. 205–233.

Savko, K.A., Samsonov, A.V., Sal'nikova, E.B., et al., HT/LP metamorphic zoning in the eastern Voronezh crystalline massif: age and parameters of metamorphism and its geodynamic environment, *Petrology,* 2015, vol. 23, no. 6, pp. 559–575.

Savko, K.A., Samsonov, A.V., Kotov, A.B., et al., The early Precambrian metamorphic events in eastern Sarmatia, *Precambrian Res.,* 2018, vol. 311, pp. 1–23.

Shchipansky, A.A. and Kheraskova, T.N., The Volga–Don collisional orogen in the east European Craton as the Paleoproterozoic analog of the Himalayan–Tibetan orogeny, *Geodynam. Tectonophys.,* 2023, vol. 14, no. 2, p. 0692.

Shchipansky, A.A., Samsonov, A.V., Petrova, A.Yu., and Larionova, Yu.O., Geodynamics of the eastern margin of Sarmatia in the Paleoproterozoic, *Geotectonics,* 2007, vol. 41, no. 1, pp. 38–62.

Skryabin V.Yu., Savko K.A., Skryabin M.V., Terentiev R.A. Cambrian Magmatic Activation of the East European Platform, *Dokl. Earth Sci.,* 2015, vol. 463, no. 2, pp. 822–827.

Smithies, R.H., The Archaean tonalite–trondhjemite–granodiorite (TTG) series in not an analogue of Cenozoic adakite, *Earth Planet. Sci. Lett.*, 2000, vol. 182, pp. 115–125.

Sotiriou, P., Polat, A., Windley, B., and Kusky, T., Temporal variations in the incompatible trace element systematics of Archean TTGs: implications for crustal growth and tectonic processes in the early earth, *Earth-Sci. Rev.,* 2023, vol. 236, p. 104274.

Stacey, J.S. and Kramers, J.D., Approximation of terrestrial lead isotope evolution by a two stage model, *Earth Planet. Sci. Lett.,* 1975, vol. 26, pp. 207–221.

Steiger, R.H. and Jäger, H., Subcommission on geochronology: convention of the use of decay constants in geo- and cosmochronology, *Earth Planet. Sci. Lett.,* 1977, vol. 36, pp. 359–362.

Terentiev, R.A. and Savko, K.A., Paleoproterozoic high-Mg low-Ti gabbro–granite series in Eastern Sarmatia: geochemistry and formation conditions, *Russ. Geol. Geophys.,* 2016, vol. 57, no. 6, pp. 907–932.

Terentiev, R.A. and Santosh, M., Detrital zircon geochronology and geochemistry of metasediments from the Vorontsovka Terrane: implications for microcontinent tectonics, *Int. Geol. Rev.,* 2016, vol. 58, pp. 1108–1126.

Terentiev, R.A., Savko, K.A., Santosh, M., et al., Paleoproterozoic granitoids of the Losevo Terrane, East European Craton: age, magma source and tectonic implications, *Precambrian Res.,* 2016, vol. 287, pp. 48–72.

Terentiev, R.A., Savko, K.A., and Santosh, M., Paleoproterozoic evolution of the arc-back-arc system in the East Sarmatian Orogen (East European Craton): zircon SHRIMP geochronology and geochemistry of the Losevo volcanic suite, *Am. J. Sci.,* 2017, vol. 317, pp. 707–753.

Terentiev, R.A., Savko, K.A., and Santosh, M., Post-collisional two-stage magmatism in the East Sarmatian Orogen, East European Craton: evidence from the Olkhovsky ring complex, *J. Geol. Soc. London*, 2018, vol. 175, pp. 86–99.

Terentiev, R.A., Savko, K.A., Santosh, M., et al., Paleoproterozoic granitoids of the Don terrane, East-Sarmatian Orogen: age, magma source and tectonic implications, *Precambrian Res.,* 2020, vol. 346, p. 105790.

Tsuchiya, N., Kimura, J.-I., and Kagami, H., Petrogenesis of Early Cretaceous adakitic granites from the Kitakami Mountains, Japan, *J. Volcanol. Geotherm. Res.,* 2007, vol. 167, pp. 134–159.

Tsybulyaev, S.V., Savko, K.A., Samsonov, A.V., Korish, E.Kh., Paleoproterozoic OIB- and MORB-type rift volcanics of the Kursk Block, Eastern Sarmatia: petrology and geodynamics, *Petrology,* 2021, vol. 29, no. 2, pp. 114–147.

Wang, Q., McDermott, F., Xu, J.F., et al., Cenozoic K-rich adakitic volcanic rocks in the Hohxil area, northern Tibet: lower-crustal melting in an intracontinental continental setting, *Geology,* 2005, vol. 33, pp. 465–468.

Whalen, J.B., Currie, K.L., and Chappell, B.W., A type granites: geochemical characteristics, discrimination, and petrogenesis, *Contrib. Mineral. Petrol.,* 1987, vol. 95, pp. 407–419.

White, W.M. and Klein, E.M., Composition of the oceanic crust, *Treatise Geochem,* 2-nd Ed., 2014, vol. 4, no. 13, pp. 457–496.

Williams, I.S., U-Th-Pb geochronology by ion microprobe, *Applications of Microanalytical Techniques to Understanding Mineralizing Processes, Rev. Econom. Geol.,* 1998, vol. 7, pp. 1–35.

Translated by E. Kurdyukov